ICES Journal of Marine Science, 63: 401–420 (2006)
doi:10.1016/j.icesjms.2005.07.015

The influence of the lunar nodal cycle on Arctic climate

Harald Yndestad

Yndestad, H. 2006. The influence of the lunar nodal cycle on Arctic climate. – ICES Journal of Marine Science, 63: 401–420.

The Arctic Ocean is a substantial energy sink for the northern hemisphere. Fluctuations in its energy budget will have a major influence on the Arctic climate. The paper presents an analysis of the time-series for the polar position, the extent of Arctic ice, sea level at Hammerfest, Kola section sea temperature, Røst winter air temperature, and the NAO winter index as a way to identify a source of dominant cycles. The investigation uses wavelet transformation to identify the period and the phase in these Arctic time-series. System dynamics are identified by studying the phase relationship between the dominant cycles in all time-series. A harmonic spectrum from the 18.6-year lunar nodal cycle in the Arctic time-series has been identified. The cycles in this harmonic spectrum have a stationary period, but not stationary amplitude and phase. A sub-harmonic cycle of about 74 years may introduce a phase reversal of the 18.6-year cycle. The signal-to-noise ratio between the lunar nodal spectrum and other sources changes from 1.6 to 3.2. A lunar nodal cycle in all time-series indicates that there is a forced Arctic oscillating system controlled by the pull of gravity from the moon, a system that influences long-term fluctuations in the extent of Arctic ice. The phase relation between the identified cycles indicates a possible chain of events from lunar nodal gravity cycles, to long-term tides, polar motions, Arctic ice extent, the NAO winter index, weather, and climate.

Keywords: Arctic oscillation, climate oscillation, lunar nodal cycle, NAO winter index, polar motion, wavelet analysis.

Received 15 July 2004; accepted 30 July 2005.

H. Yndestad: Ålesund University College, 6025 Ålesund, Norway. Tel: +47 70 161200; fax: +47 70 161300; e-mail: harald.yndestad@hials.no.

Introduction

The ancient Greek word for bear, "Arctos", lends its name to the constellation of the Great Bear. The Arctic takes its name from this constellation, so linking the region with the constellation that makes the sky near the North Pole. Small fluctuations in this northern pole may explain the Arctic climate oscillation.

The Arctic is the area north of the Arctic Circle (66°32′N), which includes the area of the midnight sun. The cold Arctic Ocean acts as an energy sink. The sun is never high in the sky, and most of its energy is reflected back to space by snow and ice in summer. Cooled water accumulates in circulating layers. The Arctic Ocean has four layers: Arctic Surface Water; Atlantic Water; Deep Water; and Bottom Water; all have different densities and circulation patterns. Atlantic Water from the Norwegian Sea enters the Eurasian Basin through the Fram Strait and underneath the surface layer. At a level of about 200–900 m, it follows the continental slope east and north until it meets the Transpolar Drift, then returns to the Greenland Sea. The Atlantic Water residence time is about 25 years (Aagaard and Greisman, 1975; Wallace and Moore, 1985). The circulating pattern in the Arctic Ocean is most likely influenced by the circulating polar movement. Deep Water down to 2600 m from the Norwegian Sea is exchanged between the Greenland Sea and the Eurasian Basin (Nansen and Amundsen Basins). Deep Water residence time in the Eurasian Basin is estimated to be about 75 years (Bonisch and Schlosser, 1995). This 75-year residence time is the same cycle period identified in polar motion, and in the extent of ice in the Barents Sea and Greenland. In the Amundsen Basin, Bottom Water (depth >2600 m) residence time is estimated to be 290 ± 30 years (Bonisch and Schlosser, 1995). A 290-year residence time is a fourth sub-harmonic of the 75-year cycle in the upper Deep Water.

Inflow to the Arctic Ocean passes from the North Atlantic through the Barents Sea and the eastern Fram Strait, with a minor inflow from the Bering Strait. Outflow is concentrated at the Canadian Archipelago and along East Greenland. Large-scale circulation processes in the Arctic

1054-3139/$32.00

Ocean's deep Canadian Basin, Markov Basin, and Eurasian Basin all have a strong influence on southward water transmission (Carmack *et al.*, 1997; Gregor *et al.*, 1998; Rudels *et al.*, 1998). Cold Arctic water from the Eurasian Basin passes the western Fram Strait and moves into the Greenland Sea. From the Greenland Sea, the cold water continues south with the East Greenland Current and the Labrador Current. East of Newfoundland, the cold current meets the warm Atlantic drift from the south, and some water returns to the northern Atlantic Ocean. Some Atlantic drift flows into the Barents Sea, and some returns to the Eurasian Basin through the Fram Strait (Anderson *et al.*, 1994; Bonisch and Schlosser, 1995).

Izhevskii (1961, 1964) introduced a system view of interacting processes between the hydrosphere, the atmosphere, and the biosphere. He argued that the heat in the ocean is a non-homogenous flow from a warm equator to the cold pole. This flow of heat in the ocean influences atmospheric processes. Atmospheric processes are reflected in the North Atlantic Oscillation (NAO), and the NAO influences weather and climate in and around the Atlantic. A strongly positive NAO winter index will lead to stronger winds and warmer air in winter. A positive trend since 1960 increased winter temperature in the northeastern Atlantic and the North Sea, a trend shift that has led to speculation about more fundamental climate change.

The North Atlantic Oscillation may be caused by a more fundamental oscillation system. Swedish oceanographer Otto Pettersson (1848–1941) postulated that the orbit of the moon and the earth have an influence on long-period tides, climate cycles, and fluctuations of marine biomasses (Pettersson, 1905, 1914, 1915, 1930). Long-period tides have been identified in the Atlantic Ocean and in the Barents Sea. Maksimov and Smirnov (1965) and Currie (1981, 1984, 1987) analysed surface temperatures in the North Atlantic, and estimated temperature cycles close to the 18.6-year lunar nodal cycle. Loder and Garret (1978) and Royer (1989, 1993) estimated an 18.6-year temperature cycle on the east and west coast of North America. The 18.6-year nodal tide has a poleward velocity component (Maksimov and Smirnov, 1967) and amplitude that is approximately 7% of the lunar diurnal component (Neuman and Pierson, 1966) and which will influence the surface layer ocean and air temperature at high latitude (Royer, 1993; Keeling and Whorf, 1997). Maksimov and his co-workers (Maksimov and Smirnov, 1964, 1967; Maksimov and Sleptsov-Shevlevich, 1970) suggested the existence of a long-period tide in the Barents Sea. Atlantic inflow to the Barents Sea is reflected in the Kola section temperature series (Bochkov, 1982). Harmonic lunar nodal cycles of $18.6/3 = 6.2$, 18.6, and $3 \times 18.6 = 55.8$ years, have been identified in this time-series (Yndestad, 1999, 2003).

There seems to be a chain of events linking the 18.6-year lunar nodal cycle and cycles of the same period in the Barents Sea. This paper presents a wavelet spectrum analysis of the time-series from polar position, Barents Sea ice extent, sea level at Hammerfest, Kola section sea temperature, Greenland Sea ice extent, Røst winter air temperature, and the NAO winter index. Each time-series is analysed by wavelet transformation to identify its dominant cycle period and phase. The analysis identifies an 18.6-year nodal spectrum in all spectra explained by oscillating climate disturbance caused by gravity oscillation from the moon. The gravity force from the 18.6-year lunar nodal cycle influences polar position and, very likely, the circulating water in the Arctic Ocean. A stationary polar-position cycle forces the Arctic Ocean, and introduces an Arctic oscillation that interacts with the Atlantic, Arctic ice extent, and Arctic atmospheric conditions. The force from the lunar nodal spectrum is transformed into a spectrum of oscillating water circulation in which some harmonic cycles are preserved by resonance. A continuous supply of movement energy is distributed throughout circulating water in the Atlantic Ocean. In this circulating process, the Arctic Ocean and the lunar nodal tide have an influence on the Atlantic Ocean inflow to the Barents Sea, as well as fluctuations in water temperature, Arctic ice extent, air temperature, and the North Atlantic Oscillation.

Material and methods

The data series on polar position (x and y directions) is based on official data from the International Earth Rotation Service (IERS), and covers the years 1846–2002. The time-series can be found at http://hpiers.obspm.fr/eoppc/eop/eopc01/, and contains ten samples per year from 1846 to 1900, and 20 samples per year from 1900 to 2002, with the celestial pole offset represented in arc degrees. The time-series was used to analyse the 1.2-year Chandler wave. The 6-, 18-, and 74-year cycles are all identified by the annual mean value of this time-series.

The area of the Greenland Sea ice extent referred to in this paper covers the Greenland Sea, the Iceland Sea, and the Norwegian Sea bounded by 30°W, 10°E, and 80°N (Figure 1). The data are based on April values from 1864 to 1998 (Vinje, 2001). The area of the Barents Sea ice extent covers the Norwegian Sea, the Barents Sea, and the Kara Sea bounded by 10°E, 80°N, and 70°E, respectively. The data are based on April values from 1864 to 1998 (Vinje, 2001).

Russian scientists at PINRO in Murmansk have provided monthly temperature values from the upper 200 m in the Kola section along 33°30′E, from 70°30′N to 72°30′N in the Barents Sea (Bochkov, 1982). The data series from 1900 to 2001 contains quarterly values from the period 1906–1920 and monthly values from 1921, some measured and some interpolated. In this paper annual mean temperatures are analysed.

The Røst air-temperature data series has been provided by the Norwegian Meteorological Institute in Oslo. The time-series has monthly values, and for the purpose of

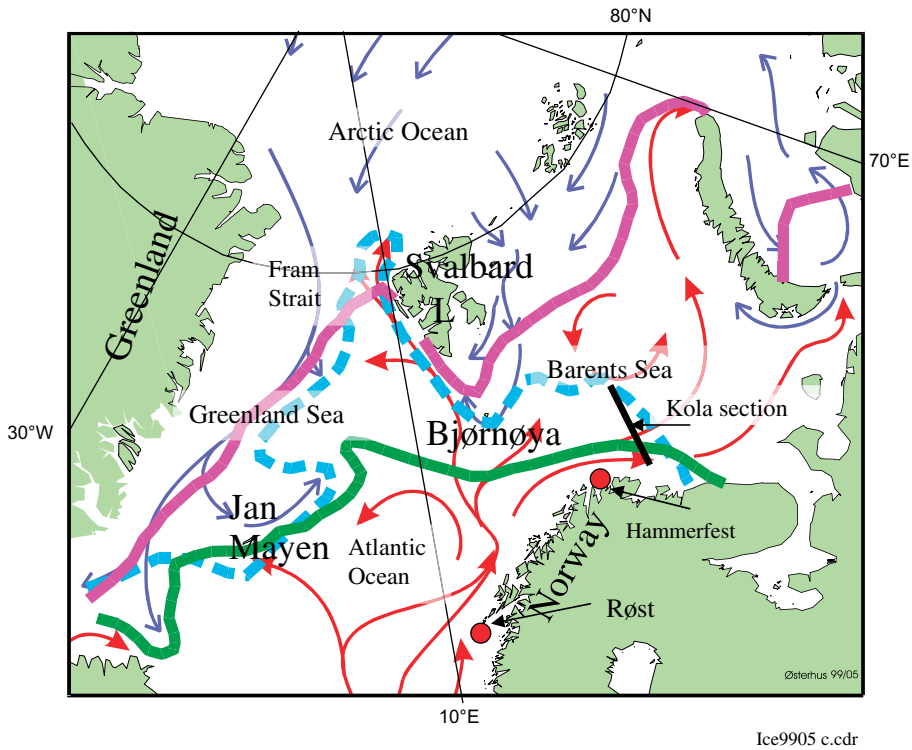

Figure 1. Study area with some ice-edge observations and ocean current patterns (after Vinje, 2001).

this analysis, winter air temperature at Røst has been computed as the mean winter temperature between December and March. The total time-series covers Røst (67°35′N 12°E) from 1880 to 1969, Skomvær (67°30′N 12°E) from 1970 to 1978, and Røst from 1979 to 1997.

The North Atlantic Oscillation (NAO) is defined as the normalized pressure difference between a station on the Azores and one on Iceland. The NAO index analysis is based on the official data from the Climate Research Unit at the University of East Anglia, UK, covers the years 1822–2001, and can be found at http://www.cru.uea.ac.uk/cru/data/nao.htm. In this analysis, the NAO winter index is computed as the mean value from December to March.

Systems theory

The climate system, $S(t)$, under investigation is represented by the simplified general system architecture:

$$S(t) = \{B(t), \{S_{\mathrm{Sun}}(t), S_{\mathrm{Moon}}(t), S_{\mathrm{Earth}}(t), S_{\mathrm{Oce}}(t), S_{\mathrm{Atm}}(t), S_{\mathrm{v}}(t)\}\}, \quad (1)$$

where $S_{\mathrm{Sun}}(t)$ represents the sun system, $S_{\mathrm{Moon}}(t)$ the moon system, $S_{\mathrm{Earth}}(t)$ the earth geo-system, $S_{\mathrm{Oce}}(t)$ the oceanographic system, and $S_{\mathrm{Atm}}(t)$ the atmospheric system. $S_{\mathrm{v}}(t)$ represents an unknown source, and $B(t)$ a time-variant mutual binding between the systems. In a system in which all subsystems are mutually related, a dominant energy source will influence the others.

Gravity effects among sun, earth, and moon result in a set of long orbital cycles that influence the tide, the polar position, and the climate on the Earth (Imbrie and Imbrie, 1980; Satterley, 1996). The lunar node is the cross-point between the moon's plane cycle and the ecliptic plane to the sun. This cross-point describes a lunar nodal cycle of 18.6134 years. The corresponding cycle of the changing inclination of the moon's orbit with respect to the earth's equatorial plane, $u_0(t)$, is described by the model

$$u_0(t) = 23°27′ + 5°09′ \sin(\omega_0 t + \varphi_0), \quad (2)$$

where $\omega_0 = 2\pi/T_0 = 2\pi/18.6134$ (rad y^{-1}) is the lunar nodal angle frequency, and time t is years 1820–2002. The cycle amplitude has a maximum in November 1987, and a minimum in March 1996 (Pugh, 1996). Therefore, the lunar nodal cycle phase is about $\varphi_0 = 0.90\pi$. The gravity force cycle from the moon introduces a horizontal and vertical 18.6-year lunar nodal tide in the Atlantic Ocean and the 18.6-year nutation of the earth's axis. The lunar-nodal tide has a harmonic and a sub-harmonic lunar-nodal spectrum that may be represented by the model

$$u(t) = \sum_n a_n(t) \sin(n\omega_0 t + \varphi_n(t)), \quad (3)$$

where $a_n(t)$ is the amplitude, and $\varphi_n(t)$ is the phase. Harmonic cycles are related to $n = 1, 2, 3, 4, \ldots, N$ and sub-harmonic cycles to $n = 1/2, 1/3, \ldots, M$ (Wood, 1986; Keeling and Whorf, 1997).

The earth's average orbital motion around the sun defines the ecliptic. At the same time, the earth's spin axis rotates around the pole of the equatorial plane. The earth's nutation is a predictable cycle of the earth's spin around its axis on a time scale of <300 years. The four dominant periods of nutation are cycles of 18.6134 years, 9.3 years, 182.6 days (half-year), and 13.7 days (half-month), but the most dominant of the four is the nutation cycle of 18.6134 years. The polar position changes in the x and y directions of the pole of ecliptic. The pole position changes from about 0.1 to 0.3 arc degrees, a displacement of some 5−15 m. This investigation examines the potential influence of the 18.6-year lunar nodal cycle on time-series.

Time-series properties

The present analysis is based on the hypothesis that the stationary 18.6-year lunar nodal cycle introduces harmonic and sub-harmonic cycles. Each stationary cycle in this lunar nodal cycle spectrum (Equation (3)) may introduce a new set of harmonic cycles. This property may be represented by the model

$$x(t) = u(t) + v(t)$$

$$u(t) = \sum_k a_k(t)\sin(k\omega_0 t + \varphi_k(t)), \tag{4}$$

where $x(t)$ is the measured time-series, $u(t)$ the sum of lunar nodal cycles, $v(t)$ the disturbance from an unknown source, and $a_k(t)$ represents the cycle amplitude. $\varphi_k(t)$ is the phase angle, and the phase angle $\omega_0 = 2\pi/T_0 = 2\pi/18.6$ (rad y^{-1}). A cycle number k may have a value $k = n_i/n_j$ where n_i and n_j represent cycle numbers in the lunar nodal spectrum (Equation (3)).

The investigation shows that interaction between two cycles may cause a phase reversal that changes the phase angle $\varphi_k(t)$ π (rad) in the analysed time-series. This phase reversal property introduces a time-variant stochastic process. The cause of this phase reversal property is unclear, but it may be explained by an amplitude modulation between two cycles that have period $1/kT_0$ and $1/T_0$. An amplitude modulation has the simple model

$$u(t) = K[1 + A\sin(\omega_0 t/k)]\sin(\omega_0 t). \tag{5}$$

The modulated signal $u(t)$ has a carrier $u_0(t) = \sin(\omega_0 t)$ and a sub-harmonic envelope $u_k(t) = A\sin(\omega_0 t/k)$. The envelope cycle will introduce a phase reversal on the carrier cycle $u_0(t)$ when $A > 1$ (Carlson, 1968).

Cycle identification

Traditional methods of spectrum analysis cannot identify cycle periods and cycle phase in time-variant stochastic processes, so in this study, the time-series have been analysed by wavelet transformation to identify the dominant cycle periods $u_k(t)$ and the time-variant phase angle $\varphi_k(t)$. The periodicity was identified by a three-step investigation. The first step was to compute the wavelet spectrum by the transformation

$$W_{a,b}(t) = \frac{1}{\sqrt{a}}\int_R x(t)\Psi\left(\frac{t-b}{a}\right)\mathrm{d}t, \tag{6}$$

where $x(t)$ is the time-series analysed, and $\Psi(\,)$ is the wavelet impulse function. $W_{a,b}(t)$ is a set of wavelet cycles, b the translation in time, and a the time-scaling parameter in wavelet transformation. The relationship between the wavelet scaling a and a sinus period T is about $T \approx 0.8a$. In this analysis, the translation $b = 0$, so the computed wavelet transformation $W_a(t)$ represents a moving correlation between $x(t)$ and the impulse function $\Psi(\,)$ over the whole time-series $x(t)$.

Coiflet wavelet function

Daubechies (1992) constructed a wavelet with $2N$ moments equal to 0, and a scaling function with $2N-1$ moments equal to 0. The Coiflet wavelet function has a symmetrical impulse that keeps a linear phase in the wavelet transformation. Figure 2 shows the Coiflet 3 wavelet function in Matlab (Matlab, 1997), the function on which this paper is based and selected after many trials on test data.

Using this wavelet transformation, it is possible to identify single, long-period cycles in short time-series. Errors at the beginning and at the end of a time-series are reduced in the following manner. The time-series are scaled in amplitude and to zero mean value by the scaling transformation

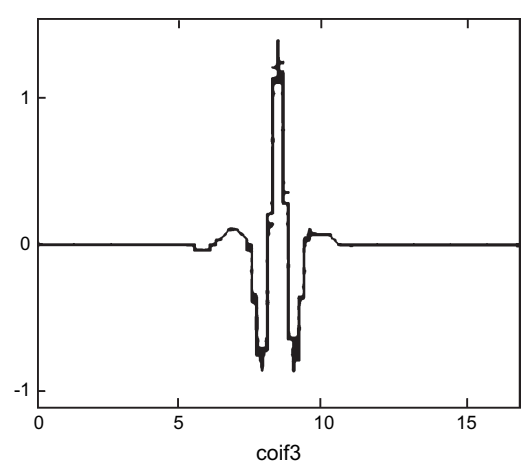

Figure 2. Coiflet 3 wavelet function.

$y(t) = [x(t) - \text{mean}(x(t))]/\text{var}(x(t))$, where $x(t)$ is the time-series, and $y(t)$ the scaled time-series. Subsequently, the time-series is expanded with symmetrical values at the beginning and end of the time-series (the 'sym' parameter in Matlab).

Time-series $x(t)$ may be represented by summing the dominant wavelets that contain most of the energy in time-series $x(t)$. The time-series may then be represented by

$$x(t) = \sum_k W_{ak}(t) + v(t) = W(t) + v(t), \quad (7)$$

where $W(t)$ represents all the dominant-wavelet cycles, and $v(t)$ is disturbance from an unknown source. A wavelet cycle represents a moving correlation between the time-series and a wavelet impulse $\Psi(\ )$ scaled by a. A single, dominant-wavelet cycle $W_{ak}(t)$ thus represents the best correlation with scale a. The dominant-wavelet cycles $W(t)$ have dominant amplitude in the wavelet spectrum.

The cycle periods of single dominant-wavelet cycles are identified by computing the autocorrelation for the wavelet spectrum $R_{aa} = E[W_a(t)W_a(t)]$. Dominant, stationary wavelet cycles have maximum values in the autocorrelation functions. The cycle period phase is identified by the optimum correlation between dominant wavelets and lunar nodal cycles by $R_k = E[W_{ak}(t)u_k(t)]$, where the phase angle $\varphi_k(t)$ is a free variable. The correlation quality is computed by the Pearson correlation coefficient

$$Q_k = R_k\sqrt{\frac{n-2}{1-R_k^2}} \sim t(n-2), \quad (8)$$

where n is the number of samples. Q_k is tested against a t-distribution by $(n-2)$ numbers of freedom to see whether the correlation is statistically significant (Daly *et al.*, 1995; Storch and Zwiers, 1999). The influence of the dominant cycles is identified by the signal-to-noise ratio between the identified dominant-wavelet cycles (Equation (7)) and disturbance from an unknown source by

$$S/N = \text{var}(W(t))/\text{var}(v(t)), \quad (9)$$

where $v(t) = (x(t) - W(t))$ is the disturbance from an unknown source.

Results

Polar position

The pole position changes in the y direction from about 0.1 to 0.3 arc degrees, which represents a displacement of about 5−15 m. The computed wavelet spectrum $W_{Pa(1:80)}(t)$ from the polar position time-series shows some dominant cycles in the wavelet spectrum (Figure 3). The identified dominant cycles have periods of about 1.2, 6, 18, and 74 years (the last three are shown in Figure 4). The identified dominant cycles are close to the temporary stationary cycles:

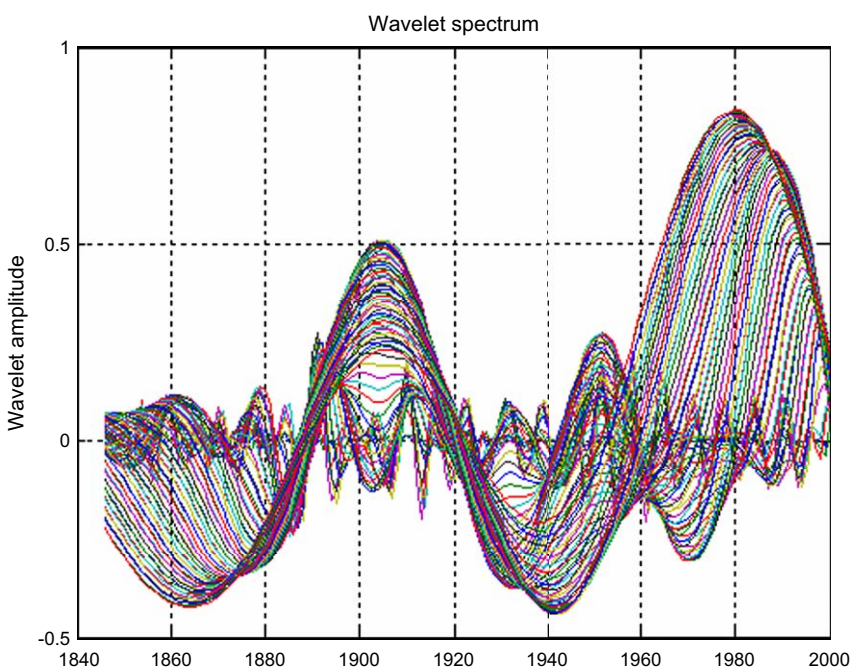

Figure 3. Wavelet spectrum $W_{P(1:80)}(t)$ of the polar position time-series in the y direction.

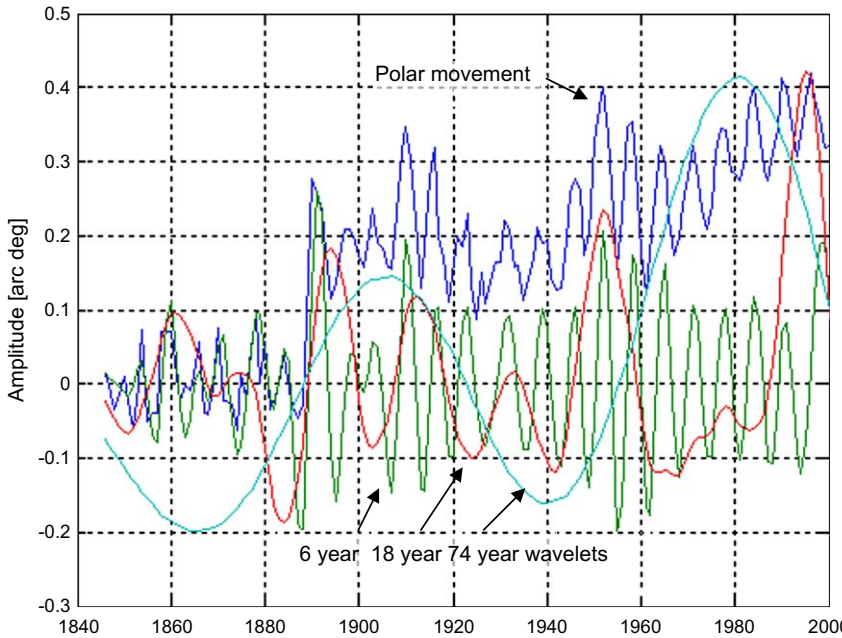

Figure 4. Polar position in the y direction time-series, 1846−2000, and estimated dominant-wavelet cycles of 74, 18, and 6 years.

$$u_{P74}(t) = a_{P74}(t)\sin(\omega_0 t/4 + 1.29\pi), \quad \text{when } t = 1846\ldots2000$$
$$u_{P18}(t) = a_{P18}(t)\sin(\omega_0 t + 0.90\pi), \quad \text{when } t = 1870\ldots1960$$
$$u_{P6}(t) = a_{P6}(t)\sin(3\omega_0 t - 1.09\pi), \quad \text{when } t = 1846\ldots2000$$
$$u_{P1.2}(t) = a_{P1.2}(t)\sin(3\times 5\omega_0 t - 1.09\pi), \quad \text{when } t = 1991\ldots1997. \tag{10}$$

These cycles represent a lunar nodal spectrum. The cross-correlation coefficients between the dominant wavelets and the stationary cycles are $R_{P74} = 0.86$, $R_{P18} = 0.70$, and $R_{P6} = 0.44$ when $t = 1846\ldots2000$ (year). The correlation values of quality are computed as $Q_{P74} = 20.5$, $Q_{P18} = 5.2$, and $Q_{P6} = 6.0$. The degrees of freedom $(n-2)$ are 153, 78, and 153. This gives a better than 95% confidence in a t-distribution, or $t(78) > 0.95$. The cross-correlation coefficient between the polar position and the dominant wavelets is estimated to be $R_{x,w} = 0.85$. The signal-to-noise ratio is estimated to be $S/N_P = 2.6$. This close correlation indicates that the gravity force from the lunar nodal cycle has a major influence on polar movement.

The cycle phase relation between the 18.6-year lunar nodal cycle is $\varphi_{L18}(t) - \varphi_{P18}(t) = (0.90\pi - 0.90\pi) = 0.0\pi$ (rad) in the period $t = 1870\ldots$ about 1960. From about 1950 to 1960, the 18-year cycle starts a π (rad) phase reversal (Figure 5). A phase difference of about 0.0π (rad) demonstrates that the 18-year polar-movement cycle $W_{P18}(t)$ is correlated in both frequency and phase to the 18.6-year lunar nodal cycle. The cycle has a phase reversal of π (rad) when the 74-year cycle has a minimum at about 1870 and 1950 (Figures 3 and 5). The phase reversal shows that the phase is controlled by the 74-year cycle. The close relationship harmonics of the lunar nodal spectrum identify the lunar nodal cycle as the energy source that influences the 18.6-year cycle of polar movement. The polar y-position state has increased step-by-step in the period from 1846 to 2000. This indicates there may be longer sub-harmonic cycles in the polar position. A wavelet analysis of polar position in the x direction has a stationary cycle of about 6.2−6.5 years. A dominant long-term cycle has maxima at about 1890, 1930, 1950, and 1980, and minima at about 1910, 1935, and 1960. This indicates a link to the 74-year cycle in the y direction.

A wavelet analysis of the polar position in the y and x directions shows a stationary cycle of about 6.2−6.5 years connected to the 1.2-year Chandler Wave. In this time-series, there is no 18-year cycle. A longer-period dominant cycle has maxima at about 1890, 1925, 1950, and 1990, and minima at about 1910, 1935, and 1965. This indicates that this cycle is related to turning points of the 74-year cycle in the y direction.

The 1.2-year wavelet cycle $W_{P1.2}(t)$ is a fifth harmonic cycle of the 6.2-year cycle. The correlation to $u_{P1.2}(t)$ is $R_{P1.2} = 0.96$ when $t = 1991.50, 1991.55\ldots1997.50$ (y). This indicates that the 1.2-year Chandler Wave cycle may be a forced harmonic cycle in the lunar nodal spectrum. The cycle difference between the estimated wavelet cycle $W_{P1.2}(t)$ and the stationary cycle $u_{P1.2}(t)$ shows a small phase delay when the 6.2-year cycle is shifted between negative and positive values. This delay may have been caused by a force delay or a synchronization of resonance between the 1.2-year and 6.2-year cycles.

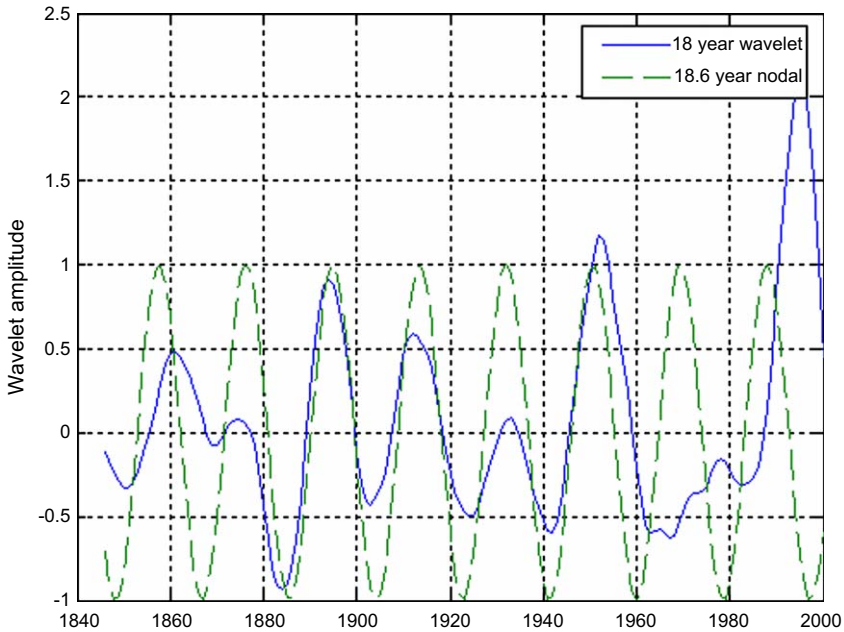

Figure 5. Identified 18-year wavelet cycle and an 18.6-year lunar nodal cycle.

Barents Sea ice extent

The Barents Sea is a mixture of cold Arctic Water from the Arctic Ocean and an inflow of warmer Atlantic Water, and its "ice-extent" time-series is a climate indicator for a large area of both the Barents Sea and the Kara Sea. The computed set of wavelets $W_{B(1:80)}(t)$ is shown in Figure 6, and the data series and dominant-wavelet cycles are depicted in Figure 7. The spectrum has dominant wavelets $W_{B6}(t)$, $W_{B18}(t)$, and $W_{B74}(t)$, which represent dominant cycles of about 6, 18, and 74 years, respectively. The identified temporary stationary dominant cycles are:

$$\begin{aligned} u_{B74}(t) &= a_{B74}(t)\sin(\omega_0 t/4 + 0.25\pi), && \text{when } t = 1864\ldots1998 \\ u_{B18}(t) &= a_{B18}(t)\sin(\omega_0 t + 0.50\pi), && \text{when } t = 1930\ldots1998 \\ u_{B6}(t) &= a_{B6}(t)\sin(3\omega_0 t + \varphi_B(6,t)), && \text{when } t = 1864\ldots1998. \end{aligned} \tag{11}$$

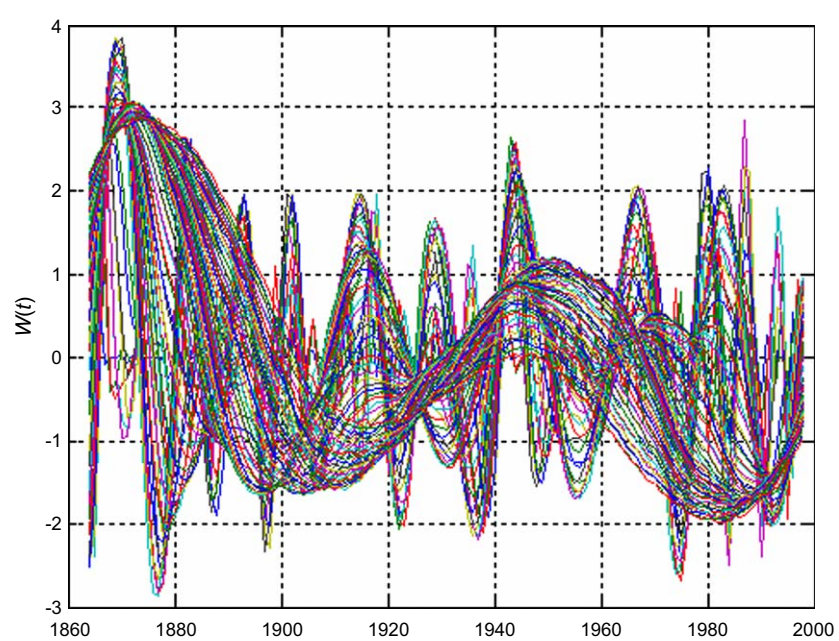

Figure 6. Wavelet spectrum $W_{B(1:80)}(t)$ of the Barents Sea ice-extent time-series.

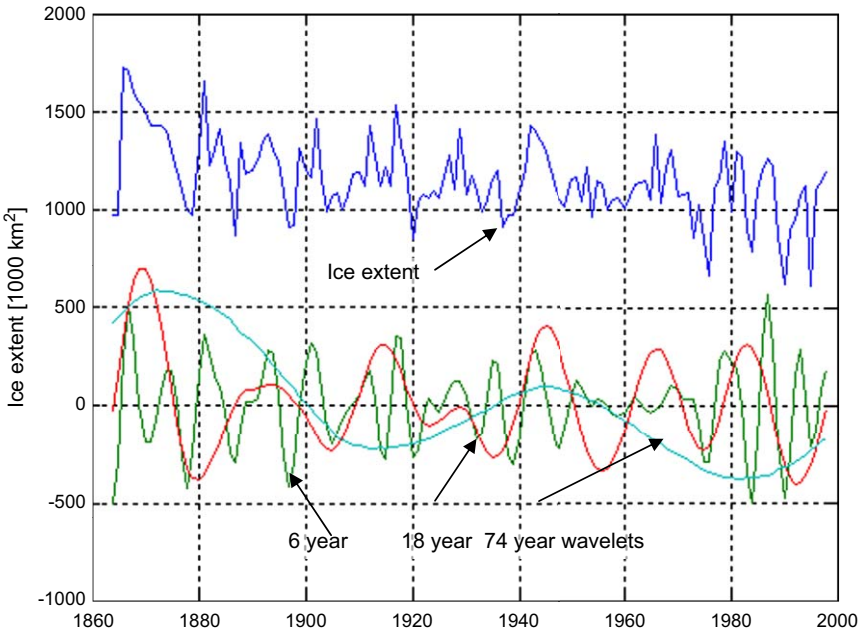

Figure 7. Time-series of Barents Sea ice extent, and dominant wavelets of 6, 18, and 74 years during the period 1864–1998.

$W_{B74}(t)$ shows a trend shift in the years 1890, 1930, and 1965, minima in 1910 and 1980, and a maximum in 1945. The cross-correlation coefficients between the dominant-wavelet cycles and the lunar nodal cycles are $R_{B74} = 0.73$ and $R_{B18} = 0.74$. The correlation values of quality are computed to be $Q_{B74} = 12.2$ and $Q_{B18} = 8.0$, with 133 degrees of freedom and $t(133) > 0.95$.

The 18-year cycle has a phase reversal in periods when the 74-year cycle $W_{B74}(t)$ has a maximum, a minimum, and a zero value. The 74-year cycle introduces a phase reversal in the 18- and 6-year cycles. The phase angle $\varphi_{B18}(t) = 1.50\pi$ (rad) in the period $t = 1895 \ldots 1930$ when $W_{B74}(t)$ has a negative period, and $\varphi_{B18}(t) = 0.50\pi$ (rad) in the period $t = 1930 \ldots 1998$ when $W_{B74}(t)$ has shifted to a positive period. The variable $\varphi_{K18}(t)$ is reversed π (rad) in the time periods $t = 1895 \ldots 1930$. The 6-year cycle has a phase reversal when the 74-year cycle reaches a minimum or a maximum, i.e. about 1870, 1815, 1945, and 1980. The 6-year cycle phase $\varphi_{B6}(t) = -0.09\pi$ (rad) in the period $t = 1980 \ldots 1998$ when the cross-correlation of $R_{B6} = 0.64$, the estimated quality value of $Q_{B6} = 3.5$ and 17 degrees of freedom. The signal-to-noise ratio is estimated to be $S/N_B = 2.0$. The cycle phase differences between the polar position and Barents Sea ice extent are:

$$\begin{aligned}
\varphi_{P74}(t) - \varphi_{B74}(t) &= (1.29\pi - 0.25\pi) = 1.04\pi\,(\text{rad}), \\
&\quad \text{when } t = 1884\ldots1998 \\
\varphi_{P18}(t) - \varphi_{B18}(t) &= (0.90\pi - 0.50\pi) = 0.40\pi\,(\text{rad}), \\
&\quad \text{when } t = 1930\ldots1998 \\
\varphi_{P6}(t) - \varphi_{B6}(t) &= (-1.09\pi - 0.09\pi) = 1.0\pi\,(\text{rad}), \\
&\quad \text{when } t = 1980\ldots1998.
\end{aligned} \tag{12}$$

The dominant 74-year cycle has a phase delay of about π (rad) compared with the same polar-position cycle. The 18-year ice-extent cycle is more closely related to the 18-year Kola cycle. As a result, the polar position is expected to be the source of the long-term 74-year oscillation in ice extent. At the same time, the 6-year and the 18-year lunar nodal tides are expected to be the source of the 6-year and the 18-year oscillations.

Kola section temperature

The Kola section time-series is an indicator of Atlantic inflow into the Barents Sea. The computed set of wavelets $W_{K(1:80)}(t)$ for the Kola temperature data series has dominant wavelets (Figure 8) at $W_{K6}(t)$, $W_{K18}(t)$, $W_{K55}(t)$, and $W_{K74}(t)$. Figure 9 shows the time-series for the period $t = 1900 \ldots 2000$ and the identified dominant-wavelet cycles of 6, 18, 55, and 74 years. A temporary stationary representation of the dominant cycles is:

$$\begin{aligned}
u_{K74}(t) &= a_{K74}(t)\sin(\omega_0 t/4 + 0.29\pi), \quad \text{when } t = 1900\ldots2000 \\
u_{K55}(t) &= a_{K55}(t)\sin(\omega_0 t/3 + 0.90\pi), \quad \text{when } t = 1900\ldots2000 \\
u_{K18}(t) &= a_{K18}(t)\sin(\omega_0 t + 0.55\pi), \quad \text{when } t = 1930\ldots2000 \\
u_{K6}(t) &= a_{K6}(t)\sin(3\omega_0 t + \varphi_{K6}(t)), \quad \text{when } t = 1900\ldots2000.
\end{aligned} \tag{13}$$

The 74-year cycle has a trend shift in 1925 and 1960, minima in 1905 and 1980, and a maximum in 1945. The cross-correlation coefficients for the long periods are $R_{K74} = 0.95$ and $R_{K55} = 0.89$, and the value of quality is estimated to be $Q_{K55} = 30.1$. There are $n - 2 = 98$ degrees of freedom and $t(98) > 0.95$.

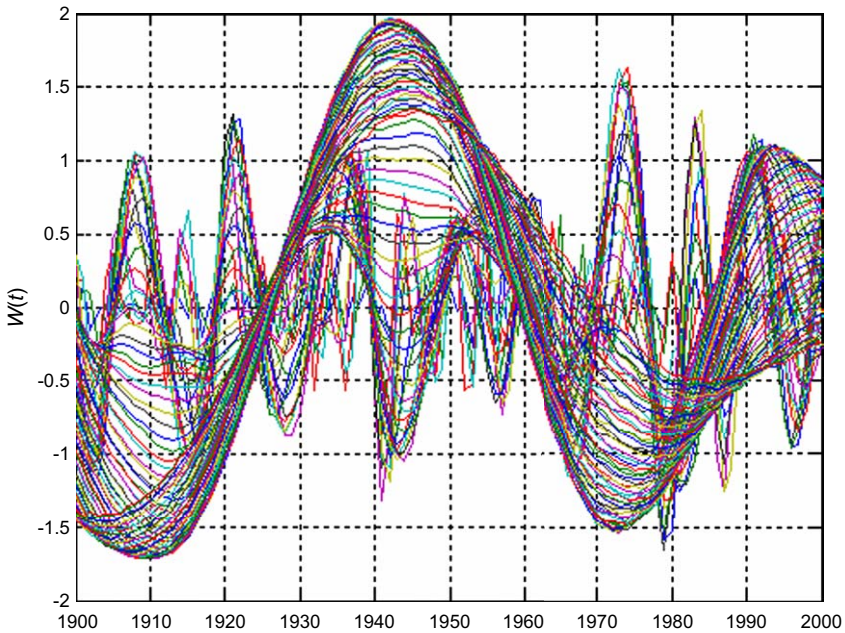

Figure 8. Wavelet spectrum of the Kola section temperature time-series.

The 74-year cycle introduces a phase reversal on the 18-year cycle. The phase angle is $\varphi_{K18}(t) = 0.55\pi$ (rad) in the period $t = 1930 \ldots 2000$, and $\varphi_{K18}(t) = 1.55\pi$ (rad) in the period $t = 1900 \ldots 1930$. There was a phase reversal when the 74-year cycle shifted from a negative to a positive state. The cross-correlation coefficient and the quality are $R_{K18} = 0.90$ and $Q_{K18} = 18.3$, respectively, when the phase of $\varphi_{K18}(t)$ is shifted in this period. The 6-year cycle has a cross-correlation coefficient of $R_{K6} = 0.4$ when $\varphi_{K6}(t) = -0.09\pi$ (rad) in the period $t = 1930 \ldots 1970$, when the 74-year cycle is in a positive state. The phase angle has a phase reversal of $\varphi_{K6}(t) = -1.09\pi$ (rad) in the period $t = 1970 \ldots 2000$ when the 74-year cycle is in a negative state. In that period, the cross-correlation

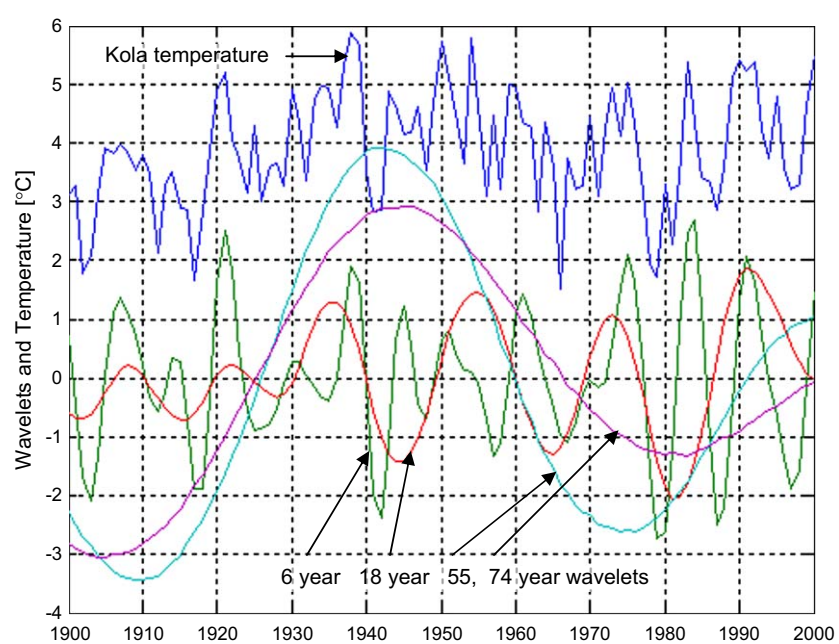

Figure 9. Kola section temperature time-series, and estimated dominant wavelets of about 6, 18, 55, and 74 years.

coefficient is estimated to be $R_{K6} = 0.37$ and $Q_{K6} = 3.9$. The signal-to-noise ratio between the wavelet sum $W_{Ka}(t) = [0.4W_{K6}(t) + 0.4W_{K18}(t) + 0.1W_{K55}(t)]$ and the unknown source $v(t) = (x_K(t) - W_{Ka}(t))$ is estimated to be $S/N_K = 3.2$. This confirms that the estimated nodal spectrum represents most of the fluctuations in the time-series.

The phase delay between the polar-position cycles and the estimated 18.6-year Kola temperature cycles are:

$$\begin{aligned}\varphi_{P74}(t) - \varphi_{K74}(t) &= (1.29\pi - 0.29\pi) = 1.00\pi\ (\text{rad})\\ \varphi_{P18}(t) - \varphi_{K74}(t) &= (0.90\pi - 0.55\pi) = 0.35\pi\ (\text{rad})\\ \varphi_{P6}(t) - \varphi_{K6}(t) &= (-1.09\pi - 0.09\pi) = 1.0\pi\ (\text{rad}).\end{aligned} \quad (14)$$

The 6-year and the 18-year cycles have a delay of about 1 year between the cycle of ice extent and the Kola section temperature. This confirms that there is less ice when there is more Atlantic inflow. The phase difference between the estimated 74-year ice-extent cycle and the Kola cycle is estimated to be about -0.04π (rad). The 74-year Kola cycle and the 74-year cycle of ice extent have the same phase. This surprising estimate suggests that the two cycles are controlled by different sources.

Mean sea level at Hammerfest

Figure 10 shows the computed wavelet spectrum $W_{H(1:30)}(t)$, and Figure 11 the time-series of the annual mean sea level at Hammerfest in the period $t = 1957 \ldots 2002$; the identified dominant-wavelet cycles are 6 and 18 years. A temporary stationary representation of the dominant cycles is:

$$\begin{aligned}u_{H18}(t) &= a_{H18}(t)\sin(\omega_0 t + 0.55\pi), \quad \text{when } t = 1957\ldots2002\\ u_{H6}(t) &= a_{H6}(t)\sin(3\omega_0 t - 0.09\pi), \quad \text{when } t = 1980\ldots1992.\end{aligned} \quad (15)$$

The cross-correlation coefficient and the correlation quality are estimated to be $R_{H18} = 0.73$ and $Q_{H18} = 6.9$, respectively, with $t(41) > 0.95$. The 6-year cycle has a phase angle $\varphi_{H6}(t) = -0.09\pi$ in the period $t = 1980 \ldots 1982$, and $\varphi_{H6}(t) = -1.09\pi$ in the period $t = 1980 \ldots 1992$. From 1957 to 1977, there was a phase reversal of π (rad) when the 18-year cycle had a minimum. The cross-correlation coefficient and the correlation quality in the total period are estimated for the 6-year cycle as $R_{H6} = 0.37$ and $Q_{H6} = 2.5$, respectively, with 41 degrees of freedom. The low correlation is related to the phase reversal in the 6-year cycle. In this period, the cross-correlation coefficient is estimated to be $R_{H6} = 0.61$, $Q_{H6} = 6.4$, and $t(41) > 0.95$. The signal-to-noise ratio between the wavelets $W_{Ha}(t) = [W_{H6}(t) + 0.9W_{H18}(t)]$, and the difference $(x_{Ha}(t) - W_{Ha}(t))$ is estimated to be $S/N_H = 1.6$. The small S/N ratio is caused by the phase reversal of the 6-year cycle.

The phase delays between the polar-position cycles and the estimated sea-level cycles at Hammerfest are:

$$\begin{aligned}\varphi_{P18}(t) - \varphi_{H18}(t) &= (0.90\pi - 0.55\pi) = 0.35\pi\\ \varphi_{P18}(t) - \varphi_{H18}(t) &= (-1.09\pi - 1.09\pi) = 0.0\pi.\end{aligned} \quad (16)$$

The phase relation between the 18-year cycles in the Hammerfest sea level and the Kola section sea temperature is

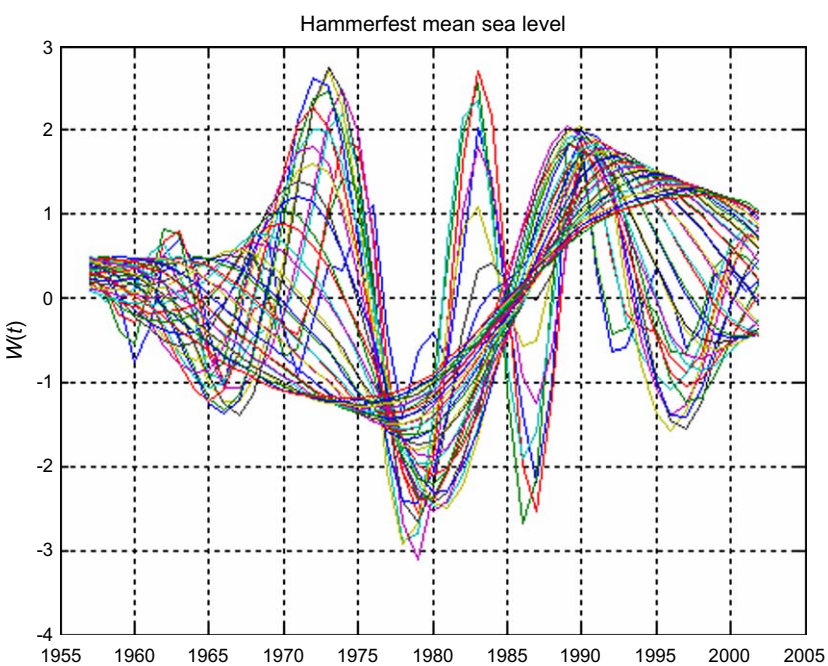

Figure 10. Wavelet spectrum from the Hammerfest annual mean sea-level time-series.

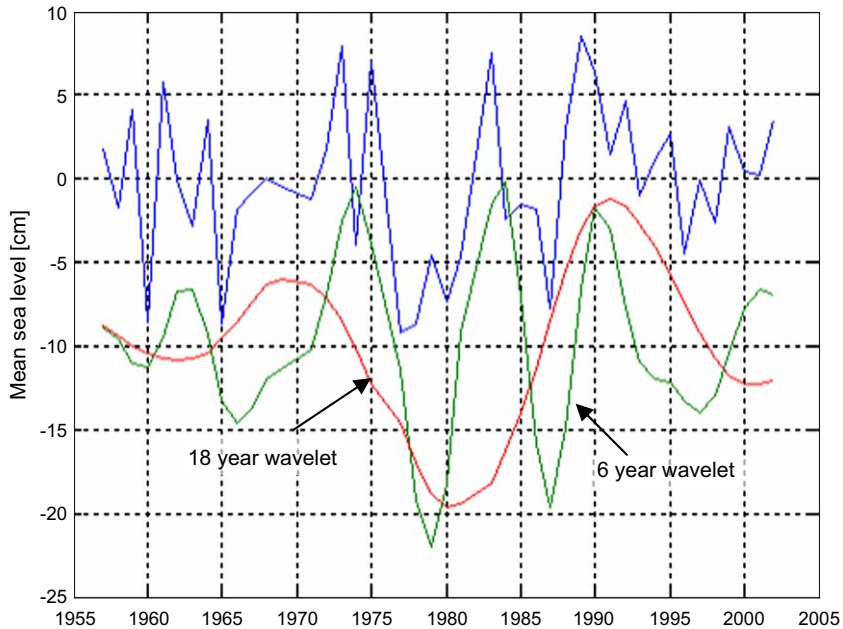

Figure 11. Hammerfest annual mean sea-level time-series, and dominant wavelets of about 6 and 18 years.

$\varphi_{Ha}(t) - \varphi_{K18}(t) = (0.55\pi - 0.55\pi) = 0.0\pi$. The closeness of this relationship shows that the long-term temperature fluctuation in the Kola section is influenced by the 18.6-year lunar nodal tide.

Greenland Sea ice extent

Greenland Sea ice covers an area between western Greenland and Svalbard, and serves as a climate indicator of outflow from the Arctic Ocean to the Greenland Sea. The computed set of wavelets $W_{G(1:80)}(t)$ of Greenland Sea ice extent has dominant cycles at about wavelet cycles $W_{G6}(t)$, $W_{G24}(t)$, and $W_{G74}(t)$, representing cycle periods of 6, 24, and 74 years, respectively. The computed wavelet spectrum is shown in Figure 12, and the full Greenland Sea ice-extent data series and dominant-wavelet cycles in Figure 13. The temporary stationary representation of the dominant cycles is:

$$\begin{aligned} u_{G74}(t) &= a_{G74}(t)\sin(\omega_0 t/4 + 1.78\pi), \quad \text{when } t = 1864\ldots1900 \\ u_{G24}(t) &= a_{G24}(t)\sin(3\omega_0 t/4 + 1.70\pi), \quad \text{when } t = 1910\ldots1980 \\ u_{G8}(t) &= a_{G8}(t)\sin(9\omega_0 t/4 + 0.38\pi), \quad \text{when } t = 1950\ldots1990. \end{aligned} \tag{17}$$

All estimated cycles are related to the $4 \times 18.6 = 74.4$ year sub-harmonic lunar nodal cycle. A cycle period of $18.6 \times 4 = 74.4$ years is the fourth sub-harmonic cycle of the 18.6-year lunar nodal cycle, and $74.4/3 = 24.8$ years is a third harmonic cycle of the 74-year cycle. The cycle period of $24.8/3 = 8.5$ years is a third sub-harmonic cycle of the 24-year cycle. The dominant 74-year wavelet cycle has a trend shift in the years 1870, 1910, 1945, and 1975, minima in 1930 and 1990, maxima in 1890 and 1960, a cross-correlation coefficient of $R_{G74} = 0.50$, a correlation value $Q_{G74} = 5.89$, and $t(133) > 0.95$. The 74-year cycle introduces a phase reversal in the 24- and 8-year cycles in the time-series. The estimated 24-year cycle $W_{G24}(t)$ has a cross-correlation coefficient $R_{G24} = 0.77$ with respect to the stationary cycle u_{G24} in the 74-year cycle period $t = 1910 \ldots 1980$. The phase is $\varphi_{G24}(t) = 0.70\pi$ (rad) in the period $t = 1864 \ldots 1910$, and $\varphi_{G24}(t) = 1.70\pi$ (rad) in the period $t = 1910 \ldots 1980$. In this estimate, the correlation-quality value is $Q_{G24} = 14.1$ and $t(65) > 0.95$. The estimated 8-year cycle $W_{G8}(t)$ shows a phase shift in 1910, 1950, and 1980 when the 74-year cycle shifted between a positive and a negative state. In the period $t = 1950 \ldots 1990$, the phase angle is about $\varphi_{G8}(t) = 0.38\pi$ (rad). In this period, the cross-correlation coefficient is $R_{G8} = 0.54$, and the quality value is estimated to be $Q_{G8} = 4.01$, with 40 degrees of freedom. The signal-to-noise ratio between the wavelet sum $W_{Ga}(t) = [100W_{G8}(t) + 60W_{G24}(t) + 60W_{G74}(t)]$ and the unknown source $v_G(t) = (x_G(t) - W_{Ga}(t))$ is calculated to be $S/N_G = 3.2$. This confirms that the estimated nodal spectrum from the 74-year cycle represents most of the fluctuations in the time-series.

The phase delay between the estimated 74-year polar-position cycle and the Greenland ice extent is $\varphi_{P74}(t) - \varphi_{G74}(t) = (1.29\pi - 1.78\pi) = 0.49\pi$ (rad). This estimate shows a delay of about 18.5 years between the 74-year cycle in the Polar position and the 74-year cycle outflow of cold Arctic water from the Arctic Ocean to the Greenland Sea.

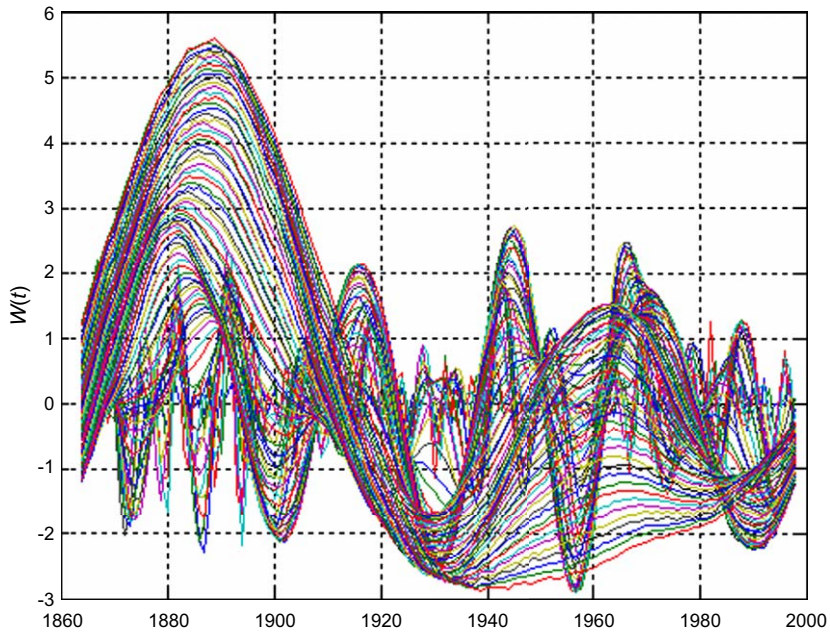

Figure 12. Wavelet spectrum from the Greenland Sea ice-extent time-series.

Røst winter temperature

Røst is a small island in the Norwegian Sea just off the Norwegian coast. The winter air temperature there is influenced by polar, Arctic winds from Greenland, via the surface of the North Atlantic, blowing towards the coast of northern Norway. The annual mean winter temperature at Røst is an indicator of cold winds from north and west.

The computed set of wavelets $W_{R(1:80)}(t)$ (Figure 14) from the Røst annual mean winter temperature has dominant wavelets at about the wavelet cycles $W_{R8}(t)$, $W_{R24}(t)$, and $W_{R74}(t)$, which represent cycles of 8, 24, and 74 years, respectively. Figure 15 shows the temperature time-series and the estimated dominant wavelets. The winter air temperature at Røst is scaled by +4 to separate the data series

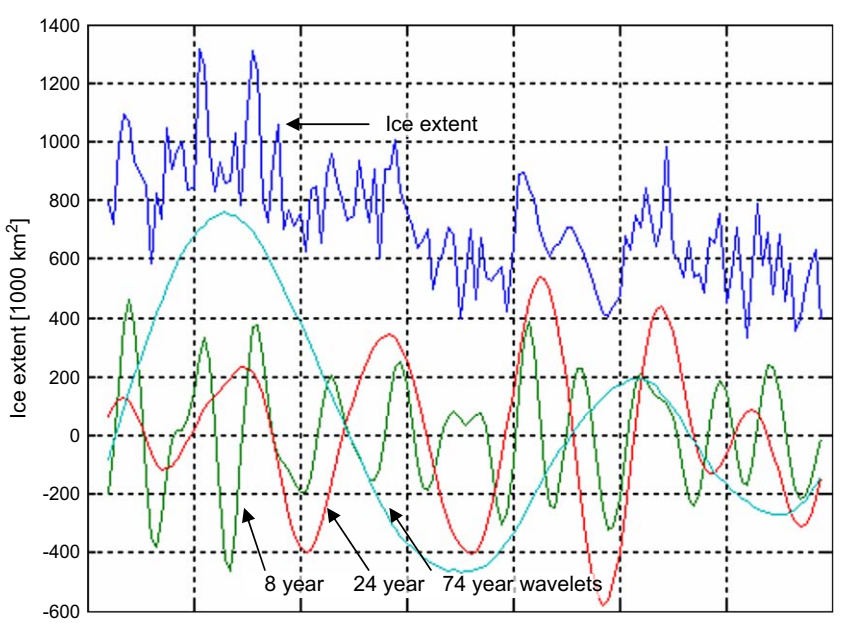

Figure 13. Greenland Sea ice-extent time-series, and identified wavelet cycles of about 6, 24, and 74 years.

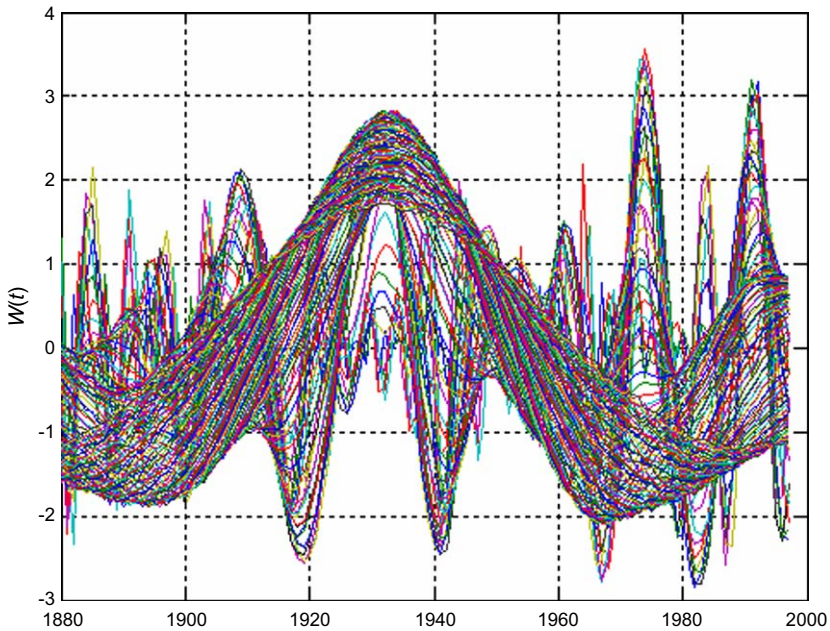

Figure 14. Wavelet spectrum from the Røst air temperature time-series.

from the estimated wavelets. The stationary representation of the dominant cycles is:

$$u_{R74}(t) = a_{R74}(t)\sin(\omega_0 t/4 + 0.51\pi), \quad \text{when } t = 1880\ldots1997$$
$$u_{R24}(t) = a_{R24}(t)\sin(3\omega_0 t/4 - 0.701\pi), \text{ when } t = 1880\ldots1910$$
$$u_{R8}(t) = a_{R8}(t)\sin(9\omega_0 t/4 - 0.382\pi), \quad \text{when} t = 1880\ldots1930. \tag{18}$$

The 74-year cycle has a trend shift at about 1910 and 1950, minima in 1900 and 1965, a maximum at about 1938, a cross-correlation coefficient of $R_{R74} = 0.92$, and a correlation value of $Q_{R74} = 24$, with $t(116) > 0.95$. This 74-year cycle controls a phase reversal in the 24- and 8-year cycles. The cross-correlation coefficient is $R_{R24} = 0.88$, with a quality value of $Q_{R24} = 11.8$ in the period $t = 1880\ldots1910$ when the 74-year cycle had

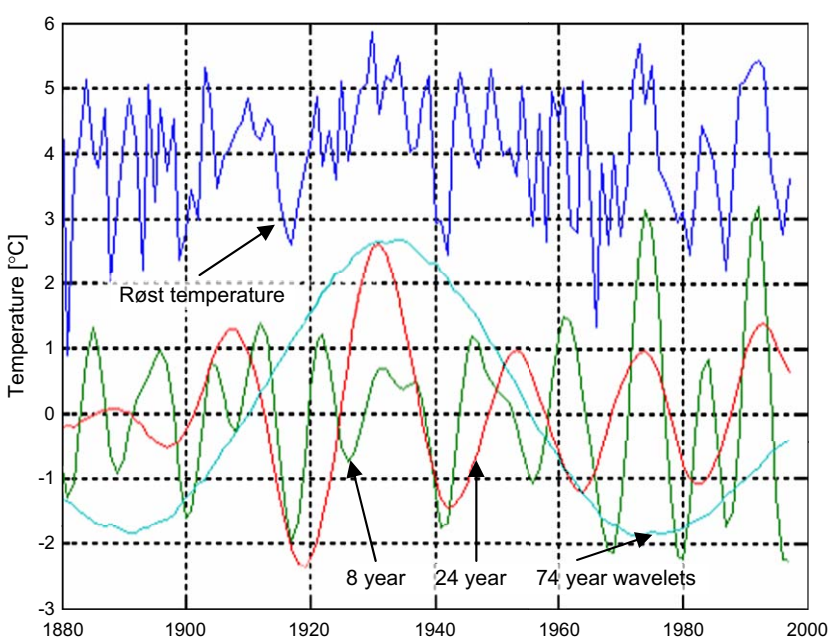

Figure 15. Røst annual mean winter air temperature time-series (+4), and the dominant wavelets of 8, 24, and 74 years.

a positive state. In that period, $t(35) > 0.95$. The cycle has a π (rad) phase reversal to $\varphi_{R24}(t) = -1.70\pi$ (rad) when the 74-year cycle had a negative state in the period $t = 1910 \ldots 1950$. The 8-year cycle has a phase of $\varphi_{R8}(t) = -0.382\pi$ (rad) in the period $t = 1880 \ldots 1930$. For that period, the cross-correlation coefficient is $R_{R8} = 0.37$, and the correlation-quality value is $Q_{R8} = 3.3$, with $t(68) > 0.95$. The cycle phase was delayed by about $\pi/2$ (rad) when the 74-year period had a maximum in 1950. The phase delay was π (rad) when the 74-year cycle was at its minimum in 1970. The signal-to-noise ratio between the dominant-wavelet sum $W_{Ra}(t) = [W_{R8}(t) + 0.5W_{R24}(t) + 0.2W_{R74}(t)]$ and the unknown source $v_R(t) = (x_R(t) - W_{Ra}(t))$ is calculated to be $S/N_R = 1.8$. This confirms that the estimated nodal spectrum from the 74-year cycle represents most of the fluctuations in the time-series.

The phase delay in the dominant Røst winter air temperature is estimated by:

$$\begin{aligned} \varphi_{P74}(t) - \varphi_{R74}(t) &= (1.29\pi - 0.51\pi) = 0.78\pi \text{ (rad)} \\ \varphi_{G24}(t) - \varphi_{R24}(t) &= (1.70\pi - 0.70\pi) = 1.0\pi \text{ (rad)}. \end{aligned} \quad (19)$$

The 24-year cycle has a phase delay of 1.0π (rad), and this is indicative of a close relationship between the increase of ice extent in the Greenland Sea and colder winter temperature at Røst. The winter temperature time-series at Røst has the same dominant cycles as estimated for the Greenland Sea ice-extent time-series. The phase delay between the 74-year NAO and Røst temperature cycles is $(1.01\pi - 0.51\pi) = 0.5\pi$ (rad). This means that the 74-year cycle at Røst moves from its maximum when the NAO 74-year cycle is headed in a negative direction.

The NAO winter index

The NAO winter index time-series has the same dominant cycles in the wavelet spectrum $W_{N(1:80)}(t)$ (Figure 16). Figure 17 shows the time-series for the NAO winter index and the estimated dominant-wavelet cycles of 6, 18, and 74 years. The NAO winter index data series in Figure 17 is scaled by +4 to separate the original data from the computed wavelets. The stationary representation of the dominant cycles is:

$$\begin{aligned} u_{N74}(t) &= a_{N74}(t)\sin(\omega_0 t/4 + 1.01\pi), && \text{when } t = 1880\ldots1997 \\ u_{N74}(t) &= a_{N74}(t)\sin(\omega_0 t + 0.48\pi), && \text{when } t = 1950\ldots2000 \\ u_{N74}(t) &= a_{N74}(t)\sin(3\omega_0 t - 0.29\pi), && \text{when } t = 1822\ldots2000. \end{aligned} \quad (20)$$

The 74-year cycle has trend shifts in 1825, 1860, 1895, 1935, and 1970, minima in 1880 and 1955, maxima in 1845, 1918, and 1995, a cross-correlation coefficient of $R_{N74} = 0.90$, and a correlation quality of $Q_{N74} = 2.4$ when $t(177) > 0.95$.

The 18-year NAO index cycle is at a maximum in the same years as the 18-year cycle of Barents Sea ice extent is at its minimum. This confirms that there is a warmer winter when there is a reduction in Arctic ice cover. The 18-year cycle has a π (rad) phase reversal at about 1840, 1890, and 1950. Then, the phase reversal is related to turning points from the 74-year cycle. The 18-year phase angle

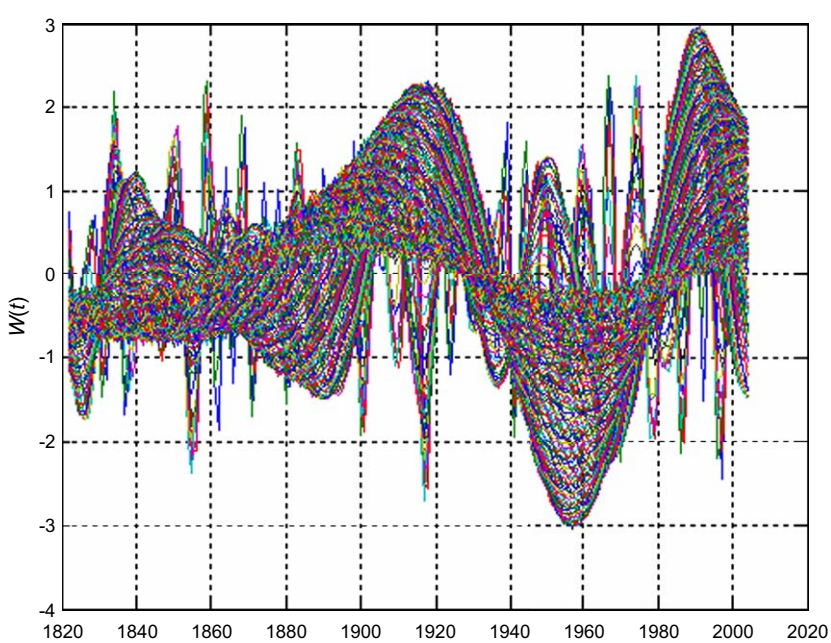

Figure 16. Wavelet spectrum from the NAO winter index time-series.

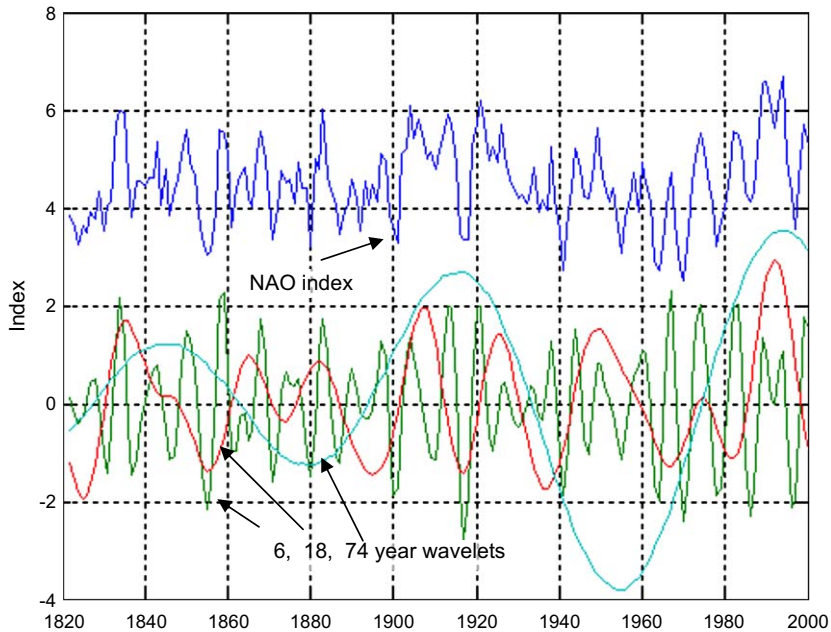

Figure 17. Time-series of the NAO winter index (+4), and the dominant-wavelet cycles of 6, 18, and 74 years.

is $\varphi_{N18}(t) = 0.48\pi$ (rad) in the period $t = 1845 \ldots 1890$, $\varphi_{N18}(t) = 1.48\pi$ (rad) in the period $t = 1890 \ldots 1950$, and $\varphi_{N18}(t) = 0.48\pi$ (rad) in the period $t = 1950 \ldots 2000$. The cross-correlation coefficient for the stationary cycle period $u_{N18}(t)$ is $R_{N18} = 0.58$ in the total period $t = 1822 \ldots 2000$ when the phase $\varphi_{N18}(t)$ is shifted. In this estimate, the correlation quality $Q_{N18} = 9.6$, and there are 177 degrees of freedom. The cross-correlation coefficient is $R_{N6} = 0.2$ when the phase angle is $\varphi_{N6}(6) = -0.29\pi$ (rad) in the period $t = 1822 \ldots 2000$. This estimate has a correlation quality of $Q_{N6} = 2.4$, and $t(177) > 0.95$. The small correlation is related to the phase control from the 74-year cycle.

The signal-to-noise ratio between the dominant wavelets $W_{Na}(t) = [W_{N8}(t) + 0.5W_{N24}(t) + 0.5W_{N74}(t)]$ and the unknown source $v_N(t) = (x_N(t) - W_{Na}(t))$ is calculated as $S/N_N = 3.0$. This confirms that the estimated nodal spectrum represents most of the fluctuations in the time-series. The phase relation with respect to polar-movement cycles is:

$$\begin{aligned} \varphi_{P74}(t) - \varphi_{N74}(t) &= (1.29\pi - 1.01\pi) = 0.28\pi \text{ (rad)} \\ \varphi_{P18}(t) - \varphi_{N18}(t) &= (0.90\pi - 0.48\pi) = 0.42\pi \text{ (rad)}. \end{aligned} \quad (21)$$

The mean phase delay between the 74-year cycle of the Barents Sea ice extent and Greenland Sea ice extent is $(\varphi_{B74}(t) + \varphi_{G74}(t))/2 = (0.25\pi + 1.78\pi)/2 = 1.01\pi$. The phase angle of the 74-year $\varphi_{N74}(t) = 1.01\pi$. This estimate shows that the 74-year cycle in the NAO winter index follows the mean long-term fluctuations of Arctic ice extent. The phase difference between the 18-year cycle in the Barents Sea ice extent and the NAO winter index is $(\varphi_{K18}(t) - \varphi_{N18}(t)) = (0.50\pi - 0.48\pi) = 0.02\pi$, or less than a year. This means that the NAO winter index is influenced by the extent of Barents Sea ice.

In 1865, the mean Barents Sea ice covered some 1 250 000 km^2, and the fluctuations were about 500 000 km^2. In 1997, the mean coverage decreased to about 750 000 km^2, but the fluctuations were still about 500 000 km^2. The mean area of fluctuation therefore increased from about 40% to 67% of total ice extent. In the same period, the fluctuation in the NAO winter index increased from about 2 to 2.5, an increase in the fluctuation of about 25%. Therefore, relatively greater fluctuation in the extent of Arctic ice introduces relatively greater disturbance in the NAO winter index. The same ratio may be a possible explanation of the increased amplitude fluctuation in the NAO winter index during the past 50 years, meaning that if Arctic ice coverage continues to fall, the amplitude of the NAO index will increase, resulting in an increase in extreme climate fluctuations.

Arctic climate cycles

Table 1 shows the lunar nodal spectrum as identified in all analysed Arctic climate indicators. In the table, the angle frequency is $\omega_0 = 2\pi/T_0 = 2\pi/18.6134$ (rad y^{-1}). This indicates that there is a stationary Arctic oscillating system controlled by the deterministic 18.6-year lunar nodal cycle.

The time-series of the polar position, Barents Sea ice extent, Kola section temperature, Hammerfest sea level, and the NAO winter index all have a dominant harmonic spectrum that is derived from a $T_0 = 18.6$-year cycle. The

Table 1. The Arctic climate cycles identified.

Climate indicator	Nodal spectrum ω_0 (rad y^{-1})	Cycle phase φ (rad)	Phase delay to polar $\Delta\varphi$ (rad)	Nodal cycle correlation R	Signal-to-noise ratio S/N
Lunar nodal cycle	ω_0	0.90π	0.00π		
Polar position	$\omega_0/4$	1.29π		0.86	2.6
	ω_0	$1.00/0.00\pi$		0.7	
	$3\omega_0$	-1.09π		0.44	
	$15\omega_0$	-1.09π		0.96	
Arctic Ocean	$\omega_0/4$				
	$3\omega_0/4$				
	$9\omega_0/4$				
Barents Sea ice extent	$\omega_0/4$	0.25π	1.04π	0.73	2
	ω_0	$1.50/0.50\pi$	0.50π	0.74	
	$3\omega_0$	$-1.09/-0.09\pi$	1.00π	0.64	
Kola section temperature	$\omega_0/4$	0.29π	1.00π	0.95	3.2
	$\omega_0/3$	0.90π		0.89	
	ω_0	$1.55/0.55\pi$	0.45π	0.9	
	$3\omega_0$	$-1.09/0.09\pi$	0.00π	0.37	
Hammerfest sea level	ω_0	0.55π	0.45π	0.73	1.6
	$3\omega_0$	$-1.09\pi/-0.09\pi$	1.0π	0.37	
Greenland Sea ice extent	$\omega_0/4$	1.78π	-0.49π	0.5	3.2
	$3\omega_0/4$	$0.70/1.70\pi$		0.77	
	$9\omega_0/4$	$1.38/0.38\pi$		0.54	
Røst winter temperature	$\omega_0/4$	0.51π	0.78π	0.92	1.8
	$3\omega_0/4$	$-1.70/-0.70\pi$		0.88	
	$9\omega_0/4$	$-1.38/-0.38\pi$		0.37	
NAO winter index	$\omega_0/4$	1.01π	0.28π	0.9	3
	ω_0	$1.48/0.48\pi$	-0.48π	0.48	
	$3\omega_0$	$-1.29/-0.29\pi$	0.2π	0.2	

Greenland Sea ice coverage and the Røst winter air temperatures have a harmonic spectrum from the sub-harmonic cycle of $4T_0 = 4 \times 18.6 = 74.4$ years. The identified cycles are clearly well correlate with the nodal reference cycles, and there is a good signal-to-noise ratio between the identified cycles and influences from other sources (Table 1). The estimates show that the cycles from the lunar nodal spectrum have a major influence on the dominant fluctuations in the time-series.

Discussion

The lunar nodal tide

The 18-year cycle of sea level identified at Hammerfest has a phase delay of about $\varphi_{H18}(t) = 0.55\pi$ (rad), a value confirmed by wavelet analysis of a number of sea-level time-series from along the Norwegian coast (unpublished data). Maksimov and Smirnov (1965, 1967) estimated a maximum lunar nodal tide at about 1950 in the Atlantic Ocean and along the Kola section. This represents a phase delay of $\varphi_{H18}(t) = 0.45\pi$ (rad), a phase distance of less than a year. However, an investigation of the temporal linkages between the Faroes–Shetland time-series and the Kola section time-series reveals a delay of about 3 years between the lunar nodal spectrum in the Faroes–Shetland time-series and the Kola temperature section time-series (Yndestad *et al.*, 2004).

Keeling and Whorf (1997) estimated strong 18-year tidal waves in 1974 and 1987 from lunar-cycle events. From those estimates, a group of 9- and 6-year tidal events were calculated, with maxima in 1965, 1974, and 1983. The same maxima and periods are identified in the Hammerfest sea-level time-series. This means that the long-term tidal cycle has a lunar nodal spectrum. The group event between a 9- and a 6-year cycle has been identified as a phase reversal of the 6-year cycle in this wavelet cycle analysis.

Polar position

Wavelet analysis of the polar position time-series in the y direction has identified lunar nodal cycles of about $4 \times 18.6 = 74.4$, 18.6, $18.6/3 = 6.2$, and $6.2/5 = 1.2$ years. The 18-year cycle has the same cycle as the earth's nutation. The earth's nutation is a 9-arc degree "wobble" of the axis of the spinning earth in a period of 18.6 years (Pugh, 1996). It is caused by gravity interaction between the earth, the sun, and the moon. The 18-year cycle has the same phase as the lunar nodal cycle, indicating that the 18-year polar movement is caused by a gravity force from

the moon and the earth's nutation. The phase reversal in 1960 shows that the 18-year cycle is influenced by the more powerful 74-year sub-harmonic cycle.

The position of the pole was stepwise displaced in the y direction in 1890 and 1960. The step came in about the same year that the 74-year Barents Sea ice cycle shifted towards a negative value, and the 74-year Greenland Sea ice coverage moved from a maximum to a negative direction. Such a connection leads to a hypothesis that long-term, stepwise displacement in the y direction can lead to greater inflow of Atlantic Water to the Arctic and long-term reduction in the coverage of Arctic ice.

Chandler (1886) demonstrated that the polar position has a wobble with a period of about 1.2 years or 435 days. The present analysis indicates that this cycle may be a forced oscillator controlled by the 6.2-year polar-movement cycle. The estimated 1.2-year polar-position cycle has a cross-correlation coefficient of $R_{P1.2} = 0.96$ to the harmonic cycle of $18.6/3 \times 5 = 6.2/5 = 1.2$ years, or 443 days. The 1.2-year cycle has a phase delay after six periods, and this introduces a mean Chandler wave period of about 6.2–6.5 years. The cause of the Chandler wobble is unclear. The stationary property of the cycle and the close relationship to a 6.2-year cycle indicate that it is a forced harmonic cycle controlled by the force of gravity from the 18.6-year lunar nodal cycle.

Arctic Ocean oscillation

Wavelet analysis of the polar position has identified a harmonic lunar nodal cycle in the y direction of about $4 \times 18.6 = 74.4$ years. This residence time represents a third harmonic cycle of the 74-year cycle, or $74.4/3 = 24.5$ years. The same cycle is estimated in the time-series of the Barents Sea ice cover, the Greenland Sea ice cover, and the winter temperature at Røst. The close relationship among these cycles may be explained by the circulating polar position that controls the residence time of circulating water in the Arctic Ocean. The circulating layers in the Arctic have residence times that are reflected in the time-series of Greenland Sea ice cover and can be explained by a "wine-glass" theory. This is based on the idea that the rotating Arctic Ocean behaves like liquid in a rotating wine glass. Accordingly, the Deep-Water oscillation has a resonance of about 74 years, a resonance related to water volume and density. A forced polar-position cycle of about 74.4 years would then control a 74-year cycle of Deep-Water circulation in the Arctic. Energy from such a forced 74-year Deep-Water oscillation would be distributed as a harmonic spectrum, in which there is a new $4 \times 74.4 \approx 290$-year resonance in the Bottom Water where the water has the most density, with a $74.4/3 \approx 25$-year resonance in the Atlantic, where the water is less dense.

The mean area of Barents Sea ice cover decreased by about 30% over the time-series. At the same time, the polar position in the y direction increased from about 0.08 to 0.35 arc degrees. This long-term motion in the pole indicates a long-term reduction in the Barents Sea ice cover that may be caused by a polar movement of longer period. Long-term displacement of the pole in a y direction may influence Arctic inflow and temperature, and the extent of Arctic Ocean ice cover.

The Barents Sea oscillation

It is generally believed that inflow of Atlantic Water to the Barents Sea is driven by atmospheric conditions (Loeng *et al.*, 1997). The lunar nodal spectrum in the polar position and the extent of Barents Sea ice cover indicate that there is a more fundamental reason for long-term Atlantic inflow. This study has shown that the lunar nodal spectrum is closely related to the annual mean sea level at Hammerfest, the Kola section temperature, and the extent of Barents Sea ice cover. Hence, the long-term inflow of Atlantic Water is controlled by long-term tides. At the same time, a close relationship has been identified between the 18-year fluctuations in the NAO winter index and the Barents Sea ice cover. This explains the close link between Barents Sea temperature and atmospheric conditions.

The 74-year Kola temperature cycle and the 74-year cycle of Barents Sea ice cover share the same cycle period and phase. This is surprising but shows that the two 74-year cycles are controlled by different sources. A potential source of the 74-year Kola temperature cycle is the Greenland Sea. There is mutual interaction of Deep Water between the Eurasian Basin, the Greenland Sea, and the Norwegian Sea. The North Atlantic's Norwegian Basin receives about a flux of some 0.95 Sv from the Greenland Sea and a flux of some 0.37 Sv from the Eurasian Basin, with the Deep-Water residence time estimated to be 31 years (Bonisch and Schlosser, 1995), or about 74.5/2 years. The Arctic flow has a phase delay of $\pi/2$ (rad) (18.6 years) from the polar movement to the Greenland Sea. A phase delay of $\pi/2$ (rad) (18.6 years) from the Greenland Sea to the Kola temperature section may have a total phase delay of π (rad) between the extent of Barents Sea ice cover and Kola section temperatures.

Greenland Sea oscillation

The extent of Greenland Sea ice cover has dominant cycles of 74 and 24 years, the same cycle periods as the residence time for Deep Water and Atlantic Water in the Arctic Ocean. The close relationship confirms that the Greenland Sea ice cover is governed by Arctic outflow. The reported salinity plume (Dickson *et al.*, 1988, 2000) in the Atlantic circulation had a trend shift in 1960, the same year that the 74-year cycle peaked and the 24-year cycle shifted trend.

The winter temperature at Røst is influenced by cold winds from the east, a fact reflected in the estimated air temperature at Røst. The Røst winter air temperature time-series has dominant cycles of 74 and 24 years, both

closely correlated with the 74- and 24-year cycles of the Greenland Sea ice cover.

NAO winter index oscillation

The NAO winter index is an important climate indicator, and this investigation has demonstrated that its dominant cycles are linked to the extent of Arctic ice cover. The influence may be explained by the fact that ice behaves as an isolator in winter between the warm sea and the cold air. The 74- and 18-year cycles identified in the NAO winter index indicate that instability in the NAO winter index increases when Arctic ice cover decreases.

The 74-year cycle in the NAO winter index represents a long-term indicator of climate change. The 74-year NAO cycle has a phase delay, exactly the mean between the 74-year cycle of Barents Sea ice cover and the 74-year cycle of Greenland Sea ice. Therefore, the total extent of Arctic ice cover is a potential source of this important 74-year climate indicator. Schlesinger and Ramankutty (1994) analysed long-term temperatures from the northern hemisphere continental regions bounding the northern Atlantic. There they found a dominant temperature cycle of about 76 years, with a maximum in 1945, the same year during which the identified 74.4-year cycle of Barents Sea ice cover was at its minimum.

The Nile flood in Egypt is an indicator of rainfall in Africa. Records from the periods 3150 BC to 2400 BC, and 622 AD to 1470 AD, show a peak with periods of 18.4, 53, and 77 years. Greenland ice cores show periodic cycles of 20, 78, and 181 years, and temperature records from central England from 1700 to 1950 show periodicities at cycles of 23 and 76 years (Borroughs, 1992; Currie, 1995). This indicates that the 74−76-year cycle is probably a long-term, stationary oscillation.

The 74-year NAO cycle explains the climate shift in 1960 and a possible new shift in the 1990s. From 2000, we may expect the 18-year NAO winter index cycle to turn positive over the next 10 years, and the 74-year cycle will turn in a negative direction during the next 30 years. This suggests perhaps a temporary period of cooler climate in the northern hemisphere. However, the long-term relationship between the step in the polar motion and the reduction in Arctic ice cover suggests that, in the long run, the climate would be expected to be warmer.

The 18-year cycle is closely correlated in both cycle period and phase to the 18-year cycle of the Barents Sea ice cover. This indicates that the 18-year cycle in the NAO winter index is influenced by the Barents Sea ice. The 74-year cycle introduces a phase reversal of the dominant cycles of 18 and 6 years, and a phase reversal of stationary cycles explains why the 18-year cycle has been difficult to estimate using traditional spectral estimate methods. The 18-year cycle has, however, been found in a number of other climate indicators, e.g. in tree rings, weather records, wine harvests, and fish catch (Currie, 1981, 1984, 1987; Currie *et al.*, 1993).

Data and methods

This analysis has some potential sources of error, which need to be stressed. There may be errors in the data samples that cannot be controlled. Single data errors or white noise should not pose a problem, because long trends are analysed, but different methods of estimating actual values are a potential source of long-term fluctuation if time-series are connected.

The wavelet analysis method is a new method of time-series analysis. Its newness raises questions about its reliability, but it must be stressed that it was developed from many trials of test data. Moreover, the coherence between the cycle periods identified and the phase in the many natural time-series shown here serves to underline the robust nature of the technique.

Coherent or chaotic

Any time-series represents a time-variant stochastic process. The stochastic process has temporary stationary cycles and time-variant phases related to phase reversals controlled by sub-harmonic cycles, meaning that we should leave linear thinking and understand the spectrum in terms of its fractal pattern.

Chaotic regime shifts are associated with long-term cycles that are difficult to predict, because they are dependent on the initial condition (Moon, 1987). This analysis has demonstrated temporary stationary cycles from the lunar nodal tide, and this leads on to new possibilities in regard to long-term prediction. At the same time, the phase reversal property reduces this long-term predictive possibility. Identifying the cause of the phase reversal may make it possible to classify the regime-shift properties. If the phase reversals are caused by free oscillating systems, chaotic regime shifts would be expected, but if they are caused by forced longer gravity from the moon, the regime shifts may be deterministic.

Why are the lunar cycles so dominant? The polar movement is only 3−15 m, and the lunar nodal tide represents only a small fraction of daily sea-level changes, so why are there dominant lunar nodal cycles in the time-series? The answer lies in the fundamental difference between stationary and random cycles. Small changes in stationary cycles have great influence when they are integrated in time and space. Hence there would not be a fixed signal-to-noise ratio: the ratio, it would increase over time and space.

Conclusion

This work has identified a harmonic spectrum from the 18.6-year lunar nodal cycle in a number of Arctic time-series. The cycles identified have a stationary cycle time, but not stationary amplitude or phase. A sub-harmonic cycle of about 74 years may introduce a phase reversal of the harmonic cycles. The high signal-to-noise ratio shows that

the lunar nodal spectrum can have a major influence on the Arctic oscillation system, which influences long-term fluctuations in the extent of Arctic ice. The lunar nodal spectrum in the coverage of Arctic ice is a potential influence on the NAO winter index, weather, and climate.

Acknowledgements

I thank Vladimir Ozhigin at the PINRO in Murmansk, for access to the Kola section temperature data series, Torgny Vinje at the Norwegian Polar Institute in Oslo, who provided the ice-extent data series, and Gudmund Anders Dalsbø of the Norwegian Meteorological Institute in Oslo, who provided the Røst data series.

References

Aagaard, K., and Greisman, P. 1975. Towards new mass and heat budgets for the Arctic Ocean. Journal of Geophysical Research, 80: 3821–3827.

Anderson, L. G., Björk, G., Holby, O., Jones, E. P., Kattner, G., Kolterman, K. B., Liljeblad, B., Lindegren, R., Rudels, B., and Swift, J. 1994. Water masses and circulation in the Eurasian Basin: results from the Oden 91 expedition. Journal of Geophysical Research, 99: 3273–3283.

Bochkov, Yu. A. 1982. Water temperature in the 0–200 m layer at the Kola Meridian in the Barents Sea, 1900–1981. Sbornik Nauchnykh Trudov, PINRO, Murmansk, 46: 113–122 (in Russian).

Bonisch, G., and Schlosser, P. 1995. Deep-water formation and exchange rates in the Greenland/Norwegian Seas and the Eurasian Basin of the Arctic Ocean derived from tracer balances. Progress in Oceanography, 35: 29–52.

Borroughs, W. J. 1992. Weather Cycles: Real or Imaginary? Cambridge University Press.

Carmack, E. C., Aagaard, K., Swift, J. H., MacDonald, R. W., McLaughlin, F. A., Jones, E. P., Perking, R. G., Smith, J. N., Ellis, K. M., and Lillius, L. R. 1997. Changes in the temperature and tracer distributions with the Arctic Ocean: results from the 1994 Arctic Ocean section. Deep Sea Research, 44: 1487–1502.

Carlson, A. B. 1968. Communication Systems. An Introduction to Signal and Noise in Electrical Communication. McGraw-Hill, London.

Chandler S. C. Jr. 1886. On a new short-period variable in Cygnus. Astronomical Journal, 7: 32.

Currie, R. G. 1981. Evidence for 18.6-year signal in temperature and drought conditions in North America since AD 1800. Journal of Geophysical Research, 86: 11055–11064.

Currie, R. G. 1984. Evidence for 18.6-year lunar nodal drought in western North America during the past millennium. Journal of Geophysical Research, 89: 1295–1308.

Currie, R. G. 1987. Examples and implications of 18.6- and 11-year terms in world weather records. *In* Climate: History, Periodicity, and Predictability. International Symposium held at Barnard College, Columbia University, New York, NY, May 1984, pp. 378–403. Ed. by M. R. Rampino, J. E. Sanders, W. S. Newman, and L. K. Konigsson. Van Nostrand Reinhold Publishing, New York. 588 pp.

Currie, R. G. 1995. Variance contribution of M_n and S_c signals to Niele River data over a 30–8-year bandwith. Journal of Coastal Research, Special Issue 17: 29–38 (Holocene Cycles: Climate, Sea Levels and Sedimentation).

Currie, R. W., Wyatt, T., and O'Brien, D. P. 1993. Deterministic signals in European fish catches, wine harvests, sea level, and further experiments. International Journal of Climatology, 8: 255–281.

Daly, F., Hand, D. J., Jones, M. C., Lunn, A. D., and McConway, K. J. 1995. Elements of Statistics. Addison-Wesley Publishing Company. ISBN 0-201-42278-6.

Daubechies, I. 1992. Ten lectures on wavelet. SIAM Journal on Mathematical Analysis, 24: 499–519.

Dickson, R. R., Meincke, J., Malmberg, S. A., and Lee, A. J. 1988. The great salinity anomality in the northern North-Atlantic, 1968–1982. Progress in Oceanography, 20: 103–151.

Dickson, R. R., Osborn, T. J., Hurrel, J. W., Meincke, J., Blindheim, J., Adlandsvik, B., Vinje, T., Alekseev, G., and Maslowski, W. 2000. The Arctic Ocean response to the North Atlantic Oscillation. Journal of Climate, 13(15): 2671–2696.

Gregor, D. J., Loeng, H., and Len, B. 1998. The influence of physical and chemical processes on containment transport into and within the Arctic. *In* AMAP Assessment Report: Arctic Pollution Issues, pp. 25–117. AMAP Secretariat.

Imbrie, John, and Imbrie, John Z. 1980. Modeling the climate response to orbital variations. Science, 207: 943–953.

Izhevskii, G. K. 1961. Oceanological Principles as Related to the Fishery Productivity of the Seas. Pishcepromizdat, Moscow. [Translated in 1966 by the Israel Program for Scientific Translations, Jerusalem]. 95 pp.

Izhevskii, G. K., 1964. Forecasting of oceanological conditions and the reproduction of commercial fish. All Union Science Research Institute of Marine Fisheries an Oceanography. Israel Program for Scientific Translations. 22 pp.

Keeling, C. D., and Whorf, T. P. 1997. Possible forcing global temperature by oceanic tides. Proceedings of the National Academy of Sciences of the United States, 94: 8321–8328.

Loder, J. W., and Garret, C. 1978. The 18.6 year cycle of the sea-surface temperature in the shallow seas due to tidal mixing. Journal of Geophysical Research, 83: 1967–1970.

Loeng, H., Ozhigin, V., and Ådlandsvik, B. 1997. Water fluxes through the Barents Sea. ICES Journal of Marine Science, 54: 310–317.

Maksimov, I. V., and Smirnov, N. P. 1964. Long-range forecasting of secular changes of the general ice formation of the Barents Sea by the harmonic component method. Murmansk Polar Science Research Institute, Sea Fisheries, 4: 75–87.

Maksimov, I. V., and Smirnov, N. P. 1965. A contribution to the study of causes of long-period variations in the activity of the Gulf Stream. Oceanology, 5: 15–24.

Maksimov, I. V., and Smirnov, N. P. 1967. A long-term circumpolar tide and its significance for the circulation of ocean and atmosphere. Oceanology, 7: 173–178 (English edition).

Maksimov, I. V., and Sleptsov-Shevlevich, B. A. 1970. Long-term changes in the tide-generation force of the moon and the icyness of the Arctic Seas. Proceedings of the N.M. Knipovich Polar Scientific-Research and Planning Institute of Marine Fisheries and Oceanography (PINRO), 27: 22–40.

Matlab. 1997. Matlab. Wavelet Toolbox. Users Guide. The Math Works Inc.

Moon, F. C. 1987. Chaotic Vibrations. John Wiley, New York. 300 pp.

Neuman, G., and Pierson, W. J. 1966. Principles of Physical Oceanography. Prentice-Hall, Englewood Cliffs, NJ. 545 pp.

Pettersson, O. 1905. On the probable occurrence in the Atlantic current of variations periodical, and otherwise, and their bearing on metrological and biological phenomena. Rapports et Procès-Verbaux des Réunions de Conseil Permanent International pour l'Exploration de la Mer, 42: 221–240.

Pettersson, O. 1914. Climatic variations in historic (*sic*) and prehistoric time: Svenska Hydrogr. Biol. Kommissiones Skrifter, 5: 26 pp.

Pettersson, O. 1915. Long periodical (*sic*) variations of the tide-generating force. Publication Circular Conseil Permanent International pour l'Exploration de la Mer, 65: 2–23.

Pettersson, O. 1930. The tidal force. A study in geophysics. Geografiska Annaler, 18: 261–322.

Pugh, D. T. 1996. Tides, Surges and Mean Sea-Level. John Wiley, New York.

Royer, T. C. 1989. Upper ocean temperature variability in the northeast Pacific: is it an indicator of global warming? Journal of Geophysical Research, 94: 175–183.

Royer, T. C. 1993. High-latitude oceanic variability associated with the 18.6-year nodal tide. Journal of Geophysical Research, 98: 4639–4644.

Rudels, B., Friedrech, H. J., and Quadfasel, D. 1998. The Arctic Circumpolar Boundary Current. Deep-Sea Research II, 46: 1023–1062.

Satterley, A. K. 1996. The Milankovitch Theory. Earth-Science Reviews, 40: 181–207.

Schlesinger, M. E., and Ramankutty, N. 1994. An oscillation in the global climate system of period 65–70 years. Nature, 367: 723–726.

von Storch, H., and Zwiers, F. W. 1999. Statistical Analysis in Climate Research. Cambridge University Press.

Vinje, T. 2001. Anomalies and trends of sea ice extent and atmospheric circulation in the Nordic Seas during the period 1864–1998. Journal of Climate, 14: 255–267.

Wallace, D. W. R., and Moore, R. M. 1985. Vertical profiles of CC13F (F-11) and CC12F2 (F-12) in the central Arctic Ocean basin. Journal of Geophysical Research, 90: 1155–1166.

Wood, F. J. 1986. Tidal Dynamics: Coastal Flooding, and Cycles of Gravitational Force. Reidel, Dordrect. 558 pp.

Yndestad, H. 1999. Earth nutation influence on the temperature regime of the Barents Sea. ICES Journal of Marine Science, 56: 381–387.

Yndestad H., 2003. A lunar-nodal spectrum in Arctic time series. ICES CM 2003/T.

Yndestad, H., Turrell, W. R., and Ozhigin, V. 2004. Temporal linkages between the Faroe-Shetland time series and the Kola section time series. ICES CM 2004/M:01. 15 pp.